Original Article

Performance of low- and high-temporal-resolution DCE-MRI texture analysis in distinguishing breast lesions from background enhancement

Yufeng Liu¹, Changliang Wang², Jianjun Wu³, Fengchun Xiao⁴, Chundan Wang⁴

¹Department of Radiology, The First Affiliated Hospital of Zhejiang Chinese Medical University (Zhejiang Provincial Hospital of Chinese Medicine), Hangzhou 310006, Zhejiang, China; ²Department of Critical Care Medicine, Sir Run Run Shaw Hospital, School of Medicine, Zhejiang University, Hangzhou 310016, Zhejiang, China; ³Department of Radiology, The Second Hospital, School of Medicine, Zhejiang University, Hangzhou 310009, Zhejiang, China; ⁴Department of Pathology, The First Affiliated Hospital of Zhejiang Chinese Medical University (Zhejiang Provincial Hospital of Chinese Medicine), Hangzhou 310006, Zhejiang, China

Received April 27, 2025; Accepted August 6, 2025; Epub August 15, 2025; Published August 30, 2025

Abstract: Objectives: To investigate the diagnostic potential of texture-based analysis of dynamic contrast-enhanced MRI (DCE-MRI) for breast lesions and background enhancement (BE). Methods: This retrospective study analyzed 62 patients who underwent preoperative high-temporal resolution DCE-MRI (1+26 phases), including 39 malignant and 23 benign lesions. A control group of 78 patients received preoperative low-temporal resolution DCE-MRI (1+5 phases), comprising 46 malignant and 32 benign lesions. All patients also underwent conventional T1WI, T2WI MRI scans, and DCE-MRI. Quantitative parameters were obtained using a two-compartment Extended Tofts model, calculating pharmacokinetic parameters: volume transfer constant (K^{trans}), rate constant (K_{pn}), extravascular extracellular volume fraction (V_s), and fractional plasma volume (V_s). Texture features based on the K^{trans} map were extracted. The region of interest for the lesion center, surrounding peripheral area, and BE was delineated. Receiver operating characteristic (ROC) analysis was used to evaluate the diagnostic performance of the K^{trans} texture features model. Results: Pharmacokinetic parameters significantly differed between high-temporal resolution and low-temporal resolution DCE-MRI (P < 0.05). In the malignant group, the average K^{trans} of the lesion area from high-temporal resolution DCE-MRI was significantly correlated with pathological grading (r = 0.400, P = 0.012). There were significant differences in the mean values of K_{eo}^{trans} , K_{eo}^{t} , V_{e}^{t} , V_{e}^{t} , V_{e}^{t} , and time to peak (TTP) between the two DCE-MRI groups across the lesion, peri-lesional, and BE areas. In the differentiation between benign and malignant lesions, ROC analysis demonstrated that high-temporal resolution DCE-MRI provided slight but significant advantages in differentiating benign and malignant lesions in the lesion center, BE areas. Conclusions: Texture analysis based on high-temporal resolution DCE-MRI may potentially improve breast cancer diagnostic performance. Specifically, combining the lesion, BE area, and K^{trans}-mean parameters contributes to the diagnosis of breast lesions, background enhancement, and the pathological grading of malignant tumors.

Keywords: Breast, magnetic resonance imaging, dynamic contrast-enhanced, texture analysis

Introduction

Breast cancer is the second leading cause of cancer-related death among women and the most common malignant tumor in women worldwide [1, 2]. In China, both the incidence and mortality of breast cancer are increasing, while the age of onset is decreasing [3, 4]. Approximately 1.6 million people are diagnosed annually, and 1.2 million succumb to the illness. Early diagnosis can reduce the overall

mortality rate of breast cancer, highlighting its importance in guiding treatment strategies.

Routine contrast-enhanced magnetic resonance imaging (CE-MRI) offers high sensitivity but low specificity, limiting its diagnostic utility. While traditional CE-MRI plays a central role in diagnosing breast pathologies due to its radiation-free nature, background enhancement (BE) may obscure lesions or contribute to false-positive readings [5-7]. In view of the heteroge-

neity of benign and malignant diseases and BE tissues, high-resolution dynamic contrastenhanced MRI (DCE-MRI) can better evaluate the tissue microenvironment and texture characteristics.

DCE-MRI can predict the biological characteristics of breast cancer, tumor environment [8-10], molecular receptor subtypes [8, 11-13], and even genomic characteristics [14, 15]. Quantitative assessment of region of interest (ROI) signal intensity, spatial structure, and other image parameters through high-throughput extraction offers diagnostic value [16, 17]. Such utility can help in the early diagnosis of breast cancers [5]. Furthermore, quantitative analysis of the gray-level co-occurrence matrix of heterogeneity may serve as an indicator of metastasis and poor prognosis [18-21]. Studies suggest that factors such as texture evaluation of vasculature, lymphatic permeation, density, and angiogenesis are correlated with disease prognosis [22]. Therefore, high-resolution DCE-MRI analysis can also aid in predicting disease prognosis [11, 23].

In a previous study by our team, we confirmed the significant value of high-temporal-resolution DCE-MRI in assessing benign and malignant BI-RADS 4 breast lesions [24]. The current study aims to investigate the application of texture analysis based on kinetic parametric maps from breast DCE-MRI, focusing on different temporal resolutions for the discrimination of benign lesions, malignant lesions, and background parenchymal enhancement.

Methods

Patients

A retrospective study was conducted on the clinical data from patients (age range, 23-79 years) with clinically suspected breast disease at the First Affiliated Hospital of Zhejiang Chinese Medical University from April 2015 to June 2017. All procedures were in accordance with the ethical standards of 1964 Helsinki declaration and its later amendments or comparable ethical standards. The Ethics Committee of the First Affiliated Hospital of Zhejiang Chinese Medical University approved this study, in which informed consent was waived due to retrospective nature.

Inclusion criteria: (1) Patients clinically suspected of having breast cancer or confirmed to have breast cancer by puncture pathology; (2) Patients who underwent MRI examination; (3) Patients who underwent breast cancer surgery and provided pathological specimens within 7 days after MRI examination; (4) Patients who completed the menstrual cycle questionnaire survey; (5) Patients with complete imaging, clinical, and follow-up data.

Exclusion criteria: (1) Pregnant or lactating patients; (2) Patients who had undergone breast-conserving surgery within the past 5 years; (3) Patients with breast prosthesis implantation; (4) Patients with contraindications for MR-enhanced examination, including unstable angina pectoris, atrial fibrillation, after coronary stent implantation, bypass surgery, or renal insufficiency (glomerular filtration rate < 60 ml/min); (5) Patients unable to complete MRI examinations due to pacemakers, stents, etc; (6) Patients whose exact pathological results could not be obtained.

According to the inclusion and exclusion criteria, 128 patients were included. Of these, 66 were excluded due to lost to follow-up, no pathological result or having other types of malignant diseases. Additionally, 78 patients who underwent preoperative low-temporal resolution DCE-MRI (1+6 phases) were included as control group. Patients who had undergone neoadjuvant chemotherapy were excluded. A patient selection flowchart is shown in **Figure**

MRI protocol

A 3.0T MR scanner (Magnetomverio, Siemens Medical Solutions, Erlangen, Germany) with a 16-channel phased-array breast coil was used to perform the DCE-MRI examination. The patient was positioned prone, with the breast naturally draped in the double coil. The following parameters were used: Turbo Inversion Recovery T2-weighted MRI (TIRM) sequence (TR = 4000 ms, TE = 70 ms, Slice thickness = 4 mm, F0V = 34 cm \times 34 cm, Matrix = 448 \times 448, Nex = 2) with cross-sectional scanning; and bilateral sagittal T2-weighted imaging (T2WI) (TR = 4650 ms, TE = 85 ms, Slice thickness = 4 mm, Layer space = 1.0 mm, F0V = 20 cm \times 20 cm, Matrix = 320 \times 224, Nex = 4).

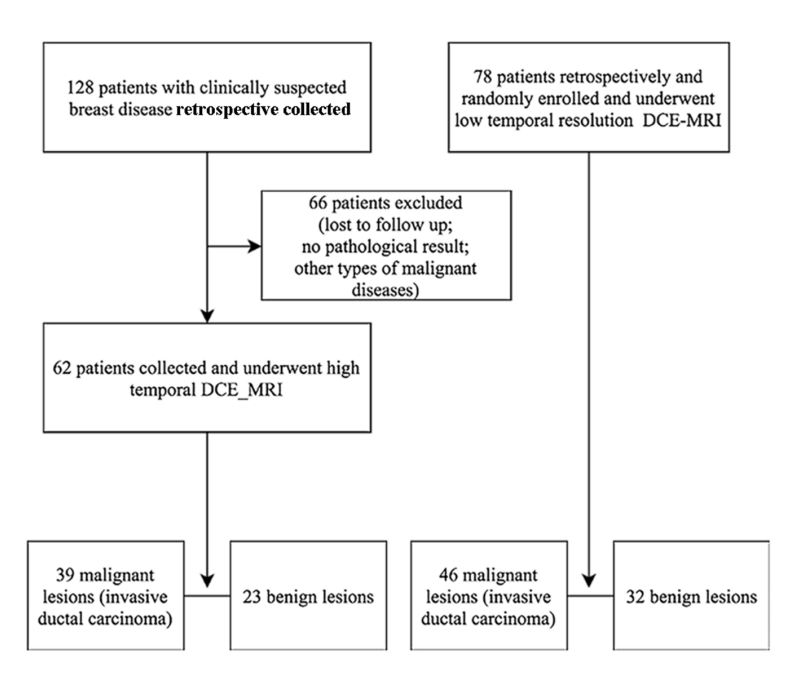


Figure 1. The patient inclusion flowchart.

A high-temporal-resolution DCE-MRI (1+26 phases) scan was conducted with the following parameters: T1 3D Dyna VIEWS, TR = 4.43 ms, TE = 1.38 ms, Slice thickness = 2 mm, FOV = 30 cm \times 30 cm, Matrix = 224 \times 224, Nex = 1, Flip angle = 15°, with a temporal resolution of 11 s and a total scanning time of 6 minutes and 3 seconds. A low-temporal-resolution DCE MRI (1+6 phases) scan was conducted with the following parameters: T1 3D Dyna VIEWS, TR = 4.51 ms, TE = 1.61 ms, Slice thickness = 1 mm, $FOV = 34 \text{ cm} \times 34 \text{ cm}$, Matrix = 448 × 448, Nex = 1, with a temporal resolution of 60 s, before the contrast injection, immediately after the start of the contrast injection, at 60 s, 120 s, 180 s. 240 s. and 300 s after injection (six acquisitions).

The contrast agent was 0.1 mmol/kg gadopentetate dimeglumine (Omniscan, GE Healthcare). A bolus injection was performed intravenously at an injection rate of 2.0 ml/sec using a double-cylinder high-pressure syringe. Following the contrast agent injection, 10 ml saline was administered.

Image analysis

All DCE-MRI image data was transferred to the Omni-Kinetic software (GE Healthcare, version 2.10) to extract K^{trans} texture features and the pharmacokinetic parameters (K^{trans} , K_{ep} , V_{e} and

V_n) for the central lesion area (Lesion), surrounding peripheral area (Peri) and background enhancement (BE) area in both the malignant and the benign groups using a two-compartment extended Tofts model and three-dimensional volume of interest. All data were analyzed by two senior radiologists (J.L. with 15 years of experience, and J.Z. with 23 years of experience in breast MRI). In cases of disagreement between the radiologists, they discussed and reached an agreement.

The ROIs were manually selected and delineated based on enhanced T1-weighted images and the pharmacokinetic maps. In **Figure 2**, both benign

and malignant lesions were clearly shown, and a polygon ROI was drawn manually to encompass the Lesion, Peri and BE area (normal breast background parenchyma enhancement), avoiding the necrotic areas and vascular beds.

Hemodynamic parameters included K^{trans} (ml/min, endothelial transfer constant, representing the rate of blood leakage to the extravascular extracellular fluid gap (EES)), $K_{\rm ep}$ (ml/min, reflux rate constant, referring to the blood leakage rate from EES back into the blood vessels), $V_{\rm e} = K^{\rm trans}/K_{\rm ep}$ (ml/ml, fractional EES volume, referring to the fraction of the EES occupied by contrast agents), and $V_{\rm p}$ (ml/ml, fractional plasma volume, referring to the plasma volume of contrast agent). These parameters were used to quantitatively evaluate the microcirculation characteristics of the lesions.

Texture feature analysis involved image conversion and quantitative analysis. For each patient, all texture features were obtained based on the K^{trans} map from DCE-MRI images. Texture feature analysis based on high-resolution DCE-MRI included the first-order distribution statistics, gray-level co-occurrence matrix (GLCM), and gray-level run-length matrix (GLRLM).

First-order distribution statistics included energy, skew, maximum, median, mean, mean

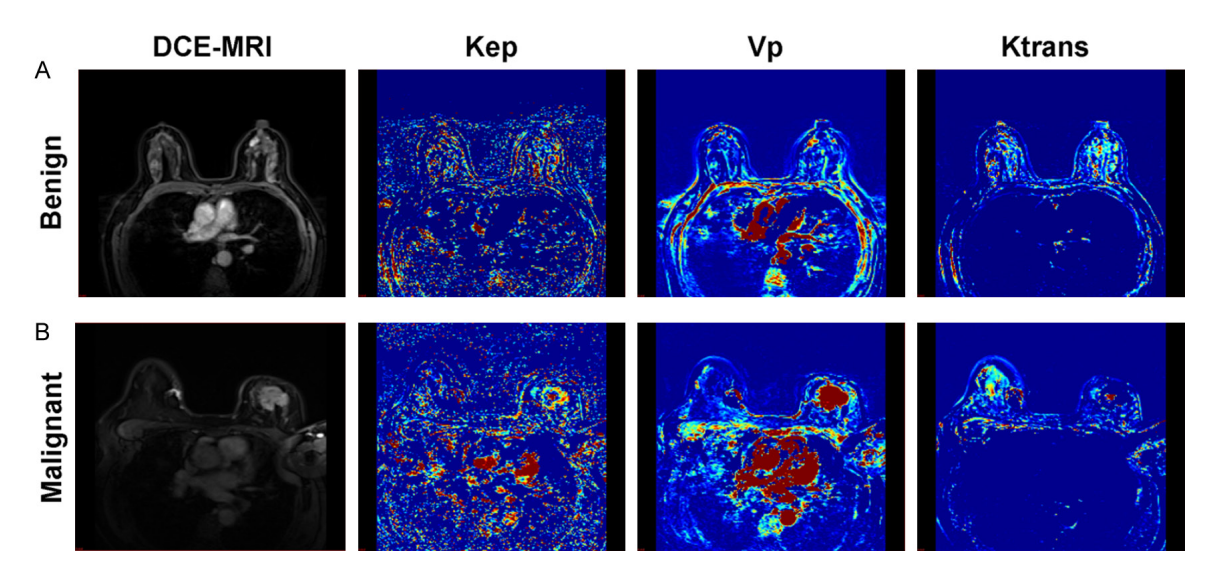


Figure 2. DCE-MRI image of typical benign and malignant lesions. A: A benign lesion identified from the high-temporal-resolution DCE-MRI; B: A malignant lesion identified from the high-temporal-resolution DCE-MRI. K^{trans} , K_{ep} , and V_p values of quantitative parameters of dynamic enhancement measured on pseudo-color maps. Pseudo-color image, with red and yellow areas showing local occupation. Blue indicates a low signal, red indicates a high signal, blue-green is a slightly lower signal, and yellow is a slightly higher signal.

absolute deviation, range, root mean square, standard deviation, and variance etc. The graylevel histogram is a discrete function of image gray level (formula: H(i) = ni/N(I = 0, 1, ..., L-1), where i represents the grayscale level, L represents the number of grayscale categories, n represents the number of pixels with grayscale level i, and N represents the total number of pixels in the image). This reflects to the probability of occurrence of pixels in the image with grayscale i. GLCM is a statistical method that describes texture, local mode, randomness, and spatial statistical characteristics, representing regional consistency and inter-regional relativity. GLRLM is the joint probability density of two position pixels, which reflects the brightness distribution and second-order statistical characteristics of spatial distribution between pixels with the same or similar brightness.

Statistical analysis

All statistical analysis was performed using IBM SPSS Statistics software (version 19.0; BM SPSS, Chicago, 1L, USA), with statistical significance set at P < 0.05. The Student's t-test was used to compare differences in hemodynamic parameters from high-resolution and low-resolution DCE-MRI for the lesion central area, surrounding peripheral area and background enhancement in the malignant

and benign groups (multiple comparisons adjusted using the Family-wise error rate). Logistic regression was used to build models based on texture features for the diagnosis of breast lesions and background enhancing. Receiver operating characteristic (ROC) analysis was used to determine the diagnostic performance of each parameter.

Since the sample size in the benign and malignant groups were not uniform, over-sampling in the smaller group was performed using the Synthetic Minority Oversampling Technique (SMOTE). For each missing sample in the smaller group, the Euclidean distance was calculated to determine the distance from all samples in the small sample set, and the nearest neighbor was designated as K. A sampling ratio was set according to the sample imbalance ratio, determining the sampling ratio (N). For each minority sample (X), a number of samples were randomly selected from its K nearest neighbor (Xn). A new sample was generated using the formula:

$$Xnew = X + rand(0, 1) \times (\tilde{X}-X).$$

For the high-resolution DCE-MRI group, the sample size was increased from 62 to 96 cases, and for the low-resolution DCE-MRI group, the sample size was increased from 78 cases to 128 cases.

Table 1. The general characteristics of included patients

Oh a wa ata wiati a a	High-temporal-resolution DCE-MRI		Low-temporal-resolution DCE-MRI		
Characteristics	Malignant	Benign	Malignant	Benign	
Number	39	23	46	32	
Age (years)					
Median (range)	53 (31-77)	48 (25-79)	49 (32-70)	48 (23-70)	
Mean ± Standard deviation	54.1±11.4	48.0±11.4	50.0±9.0	43.5±10.5	
Pathology grade					
Grade I	5	N	5	N	
Grade II	16	N	15	N	
Grade III	18	N	26	N	

Note: N means None.

The samples were randomly divided into training and testing groups in a 0.7:0.3 ratio. To address potential correlations among the features that could affect model accuracy, we conducted a three-step dimensionality reduction process. In the first step, features with significant differences were selected using a singlefactor method; in the second step, features related to the dependent variables were selected through a general linear model; in the third step, feature dimensionality reduction was performed using the Least Absolute Shrinkage and Selection Operator (LASSO) method. After dimensionality reduction, logistic regression was used to build the model, and the classification accuracy of the test group was verified. The area under the ROC curve (AUC) was calculated. The Delong-test was used to compare the ROC curves of the models.

Results

General information of the study population

A total of 62 patients underwent preoperative high-temporal-resolution DCE-MRI (1+26 phases) scans, with 39 malignant lesions (age range: 31-77 years; average age: 54.1 years; 17 lesions in the right breast, 22 in the left) and 23 benign lesions (age range: 25-79 years; average age: 48.0 years) identified. In the control group, 78 patients underwent preoperative low-temporal-resolution DCE-MRI (1+6 phases) scans, which revealed 46 malignant lesions (age range: 32-70 years; average age: 50.0 years; 21 lesions in the right breast, 25 in the left) and 32 benign lesions (age range: 23-70 years; average age: 43.5 years). Table 1 presents the general characteristics of the study population.

Hemodynamic parameters obtained from DCE-MRI in the malignant groups

According to **Table 2**, hemodynamic characteristics obtained from high-temporal-resolution and low-temporal-resolution DCE-MRI were compared in the malignant groups. With the exception of the TTP standard value in lesion area, peri-lesion area, and BE area, significant differences were observed in the values of K^{trans}, K_{ep}, V_e, V_p and mean TTP between the two DCE-MRI groups across the Lesion, Peri, and BE areas (P < 0.05). The results indicated that the hemodynamic parameters obtained from two different temporal resolutions are statistically different.

Hemodynamic parameters obtained from DCE-MRI in the benign groups

As shown in **Table 3**, the hemodynamic characteristics obtained from high-temporal-resolution and low-temporal-resolution DCE-MRI were compared in the benign groups. There were significant differences in the mean values of K^{trans}, V_e , V_p and TTP between the two DCE-MRI groups in the BE area, and in the mean values of V_e , V_p and TTP in lesion and Peri areas (P < 0.05).

Performance of K^{trans} texture feature models based on two temporal resolution DCE-MRI for benign and malignant lesions

According to the classification model constructed using the texture features from the K^{trans} map from DCE-MRI, the AUC, accuracy, sensitivity and specificity for the high-temporal-resolution DCE-MRI (1+26 phases) group were higher than those for the low-temporal-resolution DCE-MRI (1+5 phases) group (**Table 4**).

Table 2. Hemodynamic parameters obtained from high- and low-temporal resolution DCE-MRI in the malignant cohort

Area	Hemodynamic parameters	26+1 phases (n = 39)	5+1 phases (n = 46)	t	<i>p</i> -value
Lesion Area	K ^{trans} Mean	1.88±9.51	3.38±10.94	7.020	< 0.0001
	K ^{trans} Standard	0.24±0.15	1.36±0.49	13.65	< 0.0001
	K _{ep} Mean	0.94±0.35	0.42±0.19	8.847	< 0.0001
	K _{ep} Standard	0.49±0.24	0.67±0.34	2.795	< 0.0001
	V _e Mean	0.45±0.12	0.56±0.19	3.119	0.003
	$V_{_{\rm e}}$ Standard	0.17±0.06	0.44±0.07	18.86	< 0.0001
	۷ _p Mean	0.02±0.02	0.64±0.22	17.44	< 0.0001
	۷ _p Standard	0.02±0.02	0.33±0.1	19.74	< 0.0001
	TTP Mean	2.81±0.76	2.43±0.61	2.559	0.012
	TTP Standard	1.06±0.23	1.12±0.17	1.582	0.117
Peri area	K ^{trans} Mean	0.14±0.07	1.59±0.86	10.64	< 0.0001
	K ^{trans} Standard	0.15±0.1	1.57±0.45	19.08	< 0.0001
	K _{ep} Mean	0.41±0.14	0.3±0.17	3.459	0.001
	K _{eo} Standard	0.53±0.27	0.68±0.3	2.144	0.035
	V _e Mean	0.34±0.14	0.35±0.12	0.504	0.616
	V _e Standard	0.29±0.06	0.45±0.04	14.56	< 0.0001
	V _p Mean	0.02±0.02	0.4±0.16	15.11	< 0.0001
	V _p Standard	0.03±0.02	0.41±0.07	30.83	< 0.0001
	TTP Mean	3.63±0.48	2.85±0.39	8.328	< 0.0001
	TTP Standard	1.23±0.33	1.34±0.24	1.722	0.089
BE area	K ^{trans} Mean	0.04±0.05	1.7±1.14	9.003	< 0.0001
	K ^{trans} Standard	0.03±0.03	1.31±0.56	14.71	< 0.0001
	K _{ep} Mean	0.25±0.16	0.34±0.2	2.196	0.031
	K _{ep} Standard	0.26±0.16	0.62±0.3	6.764	< 0.0001
	V _e Mean	0.19±0.17	0.47±0.18	7.553	< 0.0001
	V _e Standard	0.18±0.09	0.45±0.07	15.73	< 0.0001
	V _p Mean	0±0.01	0.46±0.2	14.44	< 0.0001
	۷ Standard	0.01±0.01	0.37±0.09	26.42	< 0.0001
	TTP Mean	3.78±0.76	3.05±0.43	0.525	< 0.0001
	TTP Standard	0.95±0.44	1.06±0.2	1.424	0.158

Note: Lesion: Breast lesion central area, Peri: Surrounding peripheral lesion area, BE: Background parenchyma enhancement area; Multi-correction using Family-wise-error.

ROC curve analysis revealed the following values for the AUC, accuracy, sensitivity, and specificity of the models based on K^{trans} texture features from high-temporal-resolution DCE-MRI for benign and malignant lesions: For the central area: AUC = 0.889, accuracy = 0.867, sensitivity = 0.867, specificity = 0.933; For the background enhancement area: AUC = 0.760, accuracy = 0.700, sensitivity = 0.667, specificity = 0.867; For the (Lesion + BE) area: AUC = 0.933, accuracy = 0.800, sensitivity = 0.800, specificity = 0.933.

ROC curves (**Figure 3**) for the models based on the K^{trans} texture features obtained from low-temporal-resolution DCE-MRI for benign and

malignant lesions showed the following values: For the central area: AUC = 0.850, accuracy = 0.750, sensitivity = 0.800, specificity = 0.800; For the background enhancement: AUC = 0.716, accuracy = 0.733, sensitivity = 0.667, specificity = 0.800; For the (Lesion + BE) area: AUC = 0.868, accuracy = 0.833, sensitivity = 0.900, specificity = 0.786. After performing the Delong-test to compare models between the two DCE-MRI groups, no significant difference was observed (P > 0.05).

Discussion

In this study, we conducted a retrospective study on preoperative high-temporal-resolution

Texture analysis based on breast DCE-MRI

Table 3. Hemodynamic parameters obtained from high- and low-temporal resolution DCE-MRI in the benign cohort

Area	Hemodynamic parameters	26+1 phases (n = 23)	5+1 phases (n = 32)	t	p-value
Lesion Area	K ^{trans} Mean	0.17±0.16	2.31±1.54	6.615	< 0.0001
	K ^{trans} Standard	0.07±0.07	0.95±0.4	10.12	< 0.0001
	K _{ep} Mean	0.42±0.18	0.22±0.2	3.780	0.0004
	K _{ep} Standard	0.21±0.11	0.36±0.28	2.538	0.014
	V _e Mean	0.37±0.23	0.45±0.21	1.381	0.173
	V _e Standard	0.15±0.08	0.43±0.09	11.62	< 0.0001
	۷ _p Mean	0±0.01	0.72±0.28	12.23	< 0.0001
	V _p Standard	0.01±0.01	0.23±0.14	7.831	< 0.0001
	TTP Mean	3.94±0.74	3.04±0.54	5.225	< 0.0001
	TTP Standard	0.78±0.35	0.89±0.28	1.260	0.213
Peri area	K ^{trans} Mean	0.09±0.07	1.92±1.26	6.960	< 0.0001
	K ^{trans} Standard	0.07±0.06	1.29±0.49	11.66	< 0.0001
	K _{ep} Mean	0.27±0.12	0.24±0.16	0.915	0.365
	K _{ep} Standard	0.3±0.18	0.55±0.32	3.283	0.002
	V _e Mean	0.28±0.15	0.31±0.11	0.698	0.488
	V _e Standard	0.24±0.09	0.44±0.06	10.38	< 0.0001
	V _p Mean	0.01±0.01	0.57±0.22	12.31	< 0.0001
	V _₂ Standard	0.01±0.02	0.37±0.08	21.41	< 0.0001
	TTP Mean	3.95±0.72	3.12±0.38	5.503	< 0.0001
	TTP Standard	1.01±0.48	1.1±0.31	0.809	0.422
BE area	K ^{trans} Mean	0.06±0.07	2.76±1.63	7.691	< 0.0001
	K ^{trans} Standard	0.03±0.03	0.87±0.59	6.272	< 0.0001
	K _{ep} Mean	0.26±0.19	0.3±0.3	0.559	0.579
	K _{ep} Standard	0.21±0.15	0.35±0.34	1.956	0.056
	V _e Mean	0.2±0.12	0.59±0.29	5.959	< 0.0001
	V _e Standard	0.17±0.07	0.37±0.16	5.815	< 0.0001
	V _p Mean	0±0	0.66±0.3	10.60	< 0.0001
	V _ຼ Standard	0.01±0.01	0.22±0.16	6.259	< 0.0001
	TTP Mean	4.03±0.63	3.04±0.7	5.406	< 0.0001
	TTP Standard	0.82±0.46	0.74±0.28	0.876	0.385

Note: Lesion: Breast lesion central area, Peri: Surrounding peripheral lesion area, BE: Background parenchyma enhancement area; Multi-correction using Family-wise-error.

and low-temporal-resolution DCE-MRI texture features, including the lesion central area, surrounding peripheral area, and background enhancement area. The results indicated that high-temporal-resolution DCE-MRI may be more effective than low-temporal-resolution DCE-MRI in the differentiation of breast disease from background enhancement.

Most previous studies have focused primarily on the disease itself [16, 18-21, 25-28] or the peripheral interstitial areas [11]. However, the lesion center, periphery, and background enhancement area may play a significant role in

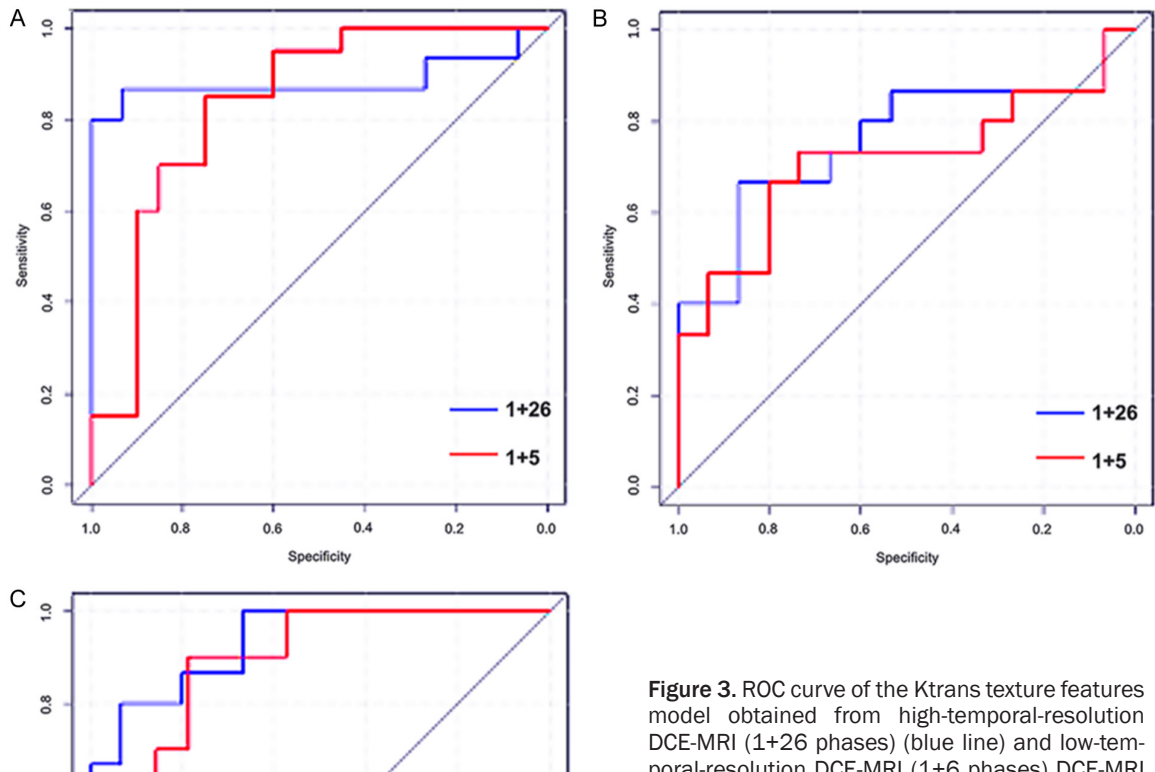
differentiating benign and malignant lesions. Few studies have comprehensively examined these areas through volume measurement. The ROI in this study included the lesion central area, surrounding peripheral area, and background enhancement area, providing a more comprehensive dataset. It was found that the hemodynamic characteristics (Ktrans, Kep, Ve, Vp, TTP) of the three ROIs, obtained from two different temporal resolution DCE-MRI scans, showed statistically significant differences. Particularly, the joint Ktrans texture features from three ROIs were useful in distinguishing benign and malignant breast lesions. These results

Texture analysis based on breast DCE-MRI

Table 4. ROC curves of K^{trans} texture feature models obtained from the high- and low-temporal-resolution DCE-MRI in differentiating malignant and benign breast lesions

ROI	AUC	95% Confidence Interval	ACC	SPC	SEN
High-resolution DCE-MRI group					
Lesion	0.889	0.759-1.000	0.867	0.933	0.867
BE	0.760	0.575-0.945	0.700	0.867	0.667
Lesion + BE	0.933	0.852-1.000	0.800	0.933	0.800
Low-resolution DCE-MRI group					
Lesion	0.850	0.725-0.975	0.750	0.800	0.800
BPE	0.716	0.518-0.913	0.733	0.800	0.667
Lesion + BE	0.868	0.723-1.000	0.833	0.786	0.900

Note: ROI: Region of interest, Lesion: Breast lesion central area, BE: Background parenchyma enhancement area, AUC: Area under the curve, ACC: Accuracy, SPC: Specificity, SEN: Sensitivity.



1+26 -1+5 1.0 0.8 0.6 0.4 0.2 0.0 Specificity

Figure 3. ROC curve of the Ktrans texture features model obtained from high-temporal-resolution DCE-MRI (1+26 phases) (blue line) and low-temporal-resolution DCE-MRI (1+6 phases) DCE-MRI (red line) in the lesion central area (Lesion, A), background enhancement (BE, B) area, and (Lesion + BE, C) area. (A) AUC values of high-temporal-resolution and low-temporal-resolution DCE-MRI in Lesion central area were 0.889 and 0.850, respectively; (B) AUC values of high-temporal-resolution and low-temporal-resolution DCE-MRI in BE area were 0.76 and 0.716, respectively; (C) AUC values of high-temporal-resolution and low-temporal-resolution DCE-MRI in (Lesion+Peri+BE) area were 0.933 and 0.868, respectively.

suggest that comprehensive measurement of the lesions and background enhancement areas can provide a more accurate diagnosis and differentiation between benign and malignant lesions.

In this study, the ROC curve showed that models from the high-temporal-resolution DCE-MRI group were slightly higher than those of the lowtemporal-resolution DCE-MRI group. This suggests that high-temporal-resolution DCE-MRI has a higher application value in the diagnosis of breast diseases. Conventional breast dynamic enhanced MRI primarily evaluates the characteristic of time signal intensity curve of breast disease (e.g., curve shape, time to peak, early enhancement rate), allowing for semiguantitative analysis of tumor characteristics. However, these semiguantitative parameters are influenced by factors such as cardiac output, imaging sequences, contrast agent injection rate, and blood flow, making them prone to errors [29]. In contrast, this study used quantitative analysis based on the Extended Tofts model, which provided multiple hemodynamic parameters, including the endothelial transfer constant of K^{trans}, reflux rate constant (K_{en}), fractional EES volume (V_e), and fractional plasma volume (V₂). The extended Tofts model is applicable to time resolution of < 12 seconds, enabling high-temporal-resolution DCE-MRI to more accurately measure lesions and detect subtle pharmacokinetic changes in tissue over very short periods. This high temporal resolution allows the sequence to accurately capture fine details, including subtle differences in contrast agent concentration. Thus, high-temporalresolution DCE-MRI can extract more texture features than low-temporal-resolution DCE-MRI, resulting in a more accurate diagnosis of breast lesions [30-32].

Although pathology remains the gold standard for disease analysis and classification, it is limited by invasiveness and localized sampling, which may cause inaccurate pathological results and restricted pathological classification of diseases. DCE-MRI, due to its noninvasive, radiation-free and high-resolution nature with soft tissue, has become an important method for diagnosing and monitoring breast diseases. In this study, we analyzed the correlation between DCE-MRI and pathological grading of malignant lesions (invasive ductal carcinoma,

IDC). The results showed that only the mean K^{trans} value in the lesion central area from high-temporal-resolution DCE-MRI was significantly correlated with pathological grade [33]. In this study, only IDC was included in the malignant group (due to the limited number of patients with other malignant types, less than 5 cases), which precluded meaningful correlation statistics for pathological grading. These findings suggest that high-temporal-resolution DCE-MRI may offer more diagnostic information in a lesion.

It was determined that the mean K^{trans} reflects the hemodynamic characteristics of the disease and is related to the number and immaturity degree of blood vessels in the central tumor and peritumor regions across different pathological grades. Tumor angiogenesis is increased in most malignant lesions, with a large number of immature blood vessels with high permeability. Therefore, low molecular weight contrast agents can enter the EES through the thin vessel walls. Previous studies also support that high-temporal-resolution DCE-MRI can more accurately evaluate the hemodynamic microenvironment of tissues, through high-throughput extracted image texture features and quantitative evaluation. For example, the gray-level co-occurrence matrix, which quantifies the enhancement of heterogeneity, has been shown to predict breast cancer invasion, prognosis, and treatment response [18-21].

Interestingly, this study found that the performance of K^{trans} texture feature models for the lesion, peripheral, and background enhancement areas based on high-temporal-resolution DCE-MRI was slightly higher than that of lowtemporal-resolution DCE-MRI. Notably, the joint texture feature model incorporating all three areas performed better than others. BE in breast tissue reflects an increase of T1 relaxation after enhancement, which directly reflects the blood supply and permeability of breast tissue. Hormones, especially estrogen, increase microvascular permeability and vasodilation in breast tissue, leading to vascular hyperplasia and ductal gland epithelial proliferation. Progesterone promotes mitosis, enhancing metabolic activity and increasing perfusion in breast tissue, which contributes to background enhancement. Tissue enhancement in MR imaging is influenced by vascular distribution,

the permeability of contrast agents, and T1 relaxation properties of the tissue [34]. In breast tissue, both the anatomy of the vascular system and the hormone effects on breast tissue play significant roles in the morphology and degree of BE [35]. High-resolution dynamic enhanced MR texture analysis can quantitatively evaluate disease and tissue heterogeneity, which is helpful for accurate assessment and early diagnosis of breast diseases and BE [5]. Thus, high-temporal-resolution DCE-MRI not only holds significant application value in the diagnosis of breast disease and background enhancement but also enables the analysis of joint texture features across the lesion and background areas.

There are several limitations in this study. First, the sample size was relatively small. The large number of texture features to be extracted and screened posed challenges due to the limited sample size, and further research with large samples is needed. Second, malignant breast lesions of other pathological types were not included in this study, which should be addressed in future studies. Third, while high-temporal-resolution DCE-MRI scans showed promising results, the protocol still needs to be further improved to optimize scanning time. Fourth, the textural features model in this study has not been validated externally. Therefore, future studies should aim for multi-center validation and incorporate clinical characteristics into the model.

Conclusions

In summary, quantitative analysis using high-temporal-resolution DCE-MRI demonstrates slightly higher application value in the diagnosis of breast lesions and background enhancement. The joint texture analysis of the lesion and BE area based on high-temporal-resolution DCE-MRI may be more helpful in diagnosis, with the mean K^{trans} contributing to the pathological grading of malignant tumors. Thus, the use of texture analysis based on high-temporal-resolution DCE-MRI has the potential to improve breast cancer diagnostic performance.

Acknowledgements

The authors thank all the medical staff who contributed to the maintenance of the medical record database. A preprint has previously been published as "Comparing Low and High-

Temporal Resolution DCE-MRI Texture Analysis for Discrimination of Breast Lesions from Background Enhancement" on Research Square (https://www.researchsquare.com/article/rs-132466/v1). This study was supported by Zhejiang Traditional Chinese Medicine Science and Technology Project (2018ZB048); Zhejiang Provincial Department of Health Platform Backbone Project (2016147237); Zhejiang Provincial Traditional Chinese Medicine Science and Technology Plan Project, 2024ZL477, a study on the precise evaluation of functional magnetic resonance imaging in the peripheral microstructure of breast cancer in different TCM syndromes based on deep learning; Zhejiang Provincial Health Department Platform Backbone Project, 2016RCA025, the value of diffusion kurtosis imaging combined with dynamic enhanced MRI in assessing the peripheral infiltration of breast cancer. The funders had roles in the design of the study, data collection, analysis, and in manuscript writing.

Disclosure of conflict of interest

None.

Abbreviations

AUC, Area under curve; BE, background enhancement; DCE-MRI, Dynamic contrastenhanced magnetic resonance imaging; EES, Extravascular extracellular space; $K_{\rm ep}$, Reflux rate constant; $K^{\rm trans}$, Endothelial transfer constant; Lesion, lesion central area; Peri, surrounding peripheral area; ROC, Receiver operating characteristic; ROI, Region of interest; $V_{\rm e}$, Fractional EES volume; $V_{\rm p}$, Fractional plasma volume.

Address correspondence to: Chundan Wang, Department of Pathology, The First Affiliated Hospital of Zhejiang Chinese Medical University (Zhejiang Provincial Hospital of Chinese Medicine), No. 54 Youdian Road, Hangzhou 310006, Zhejiang, China. Tel: +86-0571-87068001; E-mail: CdWang_HZ@163.com

References

- [1] Torre LA, Trabert B, DeSantis CE, Miller KD, Samimi G, Runowicz CD, Gaudet MM, Jemal A and Siegel RL. Ovarian cancer statistics, 2018. CA Cancer J Clin 2018; 68: 284-296.
- [2] Zhang P, Song X, Sun L, Li C, Liu X, Bao J, Tian Z, Wang X and Yu Z. A novel nomogram model of breast cancer-based imaging for predicting

- the status of axillary lymph nodes after neoadjuvant therapy. Sci Rep 2023; 13: 5952.
- [3] Li J, Chen C, Nie J, Wang L, Zhang Z and Li Y. Changes in the disease burden of breast cancer along with attributable risk factors in China from 1990 to 2019 and its projections: an analysis of the global burden of disease study 2019. Cancer Med 2023; 12: 1888-1902.
- [4] Ding R, Xiao Y, Mo M, Zheng Y, Jiang YZ and Shao ZM. Breast cancer screening and early diagnosis in Chinese women. Cancer Biol Med 2022; 19: 450-467.
- [5] Arasu VA, Miglioretti DL, Sprague BL, Alsheik NH, Buist DSM, Henderson LM, Herschorn SD, Lee JM, Onega T, Rauscher GH, Wernli KJ, Lehman CD and Kerlikowske K. Populationbased assessment of the association between magnetic resonance imaging background parenchymal enhancement and future primary breast cancer risk. J Clin Oncol 2019; 37: 954-963.
- [6] Vreemann S, Dalmis MU, Bult P, Karssemeijer N, Broeders MJM, Gubern-Mérida A and Mann RM. Amount of fibroglandular tissue FGT and background parenchymal enhancement BPE in relation to breast cancer risk and false positives in a breast MRI screening program: a retrospective cohort study. Eur Radiol 2019; 29: 4678-4690.
- [7] Romeo V, Clauser P, Rasul S, Kapetas P, Gibbs P, Baltzer PAT, Hacker M, Woitek R, Helbich TH and Pinker K. Al-enhanced simultaneous multiparametric (18)F-FDG PET/MRI for accurate breast cancer diagnosis. Eur J Nucl Med Mol Imaging 2022; 49: 596-608.
- [8] Ochoa-Albiztegui RE, Sevilimedu V, Horvat JV, Thakur SB, Helbich TH, Trattnig S, Morris EA, Reiner JS and Pinker K. Pharmacokinetic analysis of dynamic contrast-enhanced magnetic resonance imaging at 7T for breast cancer diagnosis and characterization. Cancers (Basel) 2020; 12: 3763.
- [9] Ni M, Zhou X, Liu J, Yu H, Gao Y, Zhang X and Li Z. Prediction of the clinicopathological subtypes of breast cancer using a fisher discriminant analysis model based on radiomic features of diffusion-weighted MRI. BMC Cancer 2020; 20: 1073.
- [10] Li Y, Fan Y, Xu D, Li Y, Zhong Z, Pan H, Huang B, Xie X, Yang Y and Liu B. Deep learning radiomic analysis of DCE-MRI combined with clinical characteristics predicts pathological complete response to neoadjuvant chemotherapy in breast cancer. Front Oncol 2022; 12: 1041142.
- [11] Nagasaka K, Satake H, Ishigaki S, Kawai H and Naganawa S. Histogram analysis of quantitative pharmacokinetic parameters on DCE-MRI: correlations with prognostic factors and molecular subtypes in breast cancer. Breast Cancer 2019; 26: 113-124.

- [12] Tsai WC, Chang KM and Kao KJ. Dynamic contrast enhanced MRI and intravoxel incoherent motion to identify molecular subtypes of breast cancer with different vascular normalization gene expression. Korean J Radiol 2021; 22: 1021-1033.
- [13] Leithner D, Bernard-Davila B, Martinez DF, Horvat JV, Jochelson MS, Marino MA, Avendano D, Ochoa-Albiztegui RE, Sutton EJ, Morris EA, Thakur SB and Pinker K. Radiomic signatures derived from diffusion-weighted imaging for the assessment of breast cancer receptor status and molecular subtypes. Mol Imaging Biol 2020; 22: 453-461.
- [14] Fan M, Xia P, Liu B, Zhang L, Wang Y, Gao X and Li L. Tumour heterogeneity revealed by unsupervised decomposition of dynamic contrastenhanced magnetic resonance imaging is associated with underlying gene expression patterns and poor survival in breast cancer patients. Breast Cancer Res 2019; 21: 112.
- [15] Arefan D, Chai R, Sun M, Zuley ML and Wu S. Machine learning prediction of axillary lymph node metastasis in breast cancer: 2D versus 3D radiomic features. Med Phys 2020; 47: 6334-6342.
- [16] Forghani R, Srinivasan A and Forghani B. Advanced tissue characterization and texture analysis using dual-energy computed tomography: horizons and emerging applications. Neuroimaging Clin N Am 2017; 27: 533-546.
- [17] Chen K, Yin G and Xu W. Predictive value of (18)F-FDG PET/CT-based radiomics model for occult axillary lymph node metastasis in clinically node-negative breast cancer. Diagnostics (Basel) 2022; 12: 997.
- [18] Burnside ES, Drukker K, Li H, Bonaccio E, Zuley M, Ganott M, Net JM, Sutton EJ, Brandt KR, Whitman GJ, Conzen SD, Lan L, Ji Y, Zhu Y, Jaffe CC, Huang EP, Freymann JB, Kirby JS, Morris EA and Giger ML. Using computer-extracted image phenotypes from tumors on breast magnetic resonance imaging to predict breast cancer pathologic stage. Cancer 2016; 122: 748-757.
- [19] Fan M, Zhang P, Wang Y, Peng W, Wang S, Gao X, Xu M and Li L. Radiomic analysis of imaging heterogeneity in tumours and the surrounding parenchyma based on unsupervised decomposition of DCE-MRI for predicting molecular subtypes of breast cancer. Eur Radiol 2019; 29: 4456-4467.
- [20] Kim JH, Ko ES, Lim Y, Lee KS, Han BK, Ko EY, Hahn SY and Nam SJ. Breast cancer heterogeneity: MR imaging texture analysis and survival outcomes. Radiology 2017; 282: 665-675.
- [21] Wu J, Gong G, Cui Y and Li R. Intratumor partitioning and texture analysis of dynamic contrast-enhanced (DCE)-MRI identifies relevant

Texture analysis based on breast DCE-MRI

- tumor subregions to predict pathological response of breast cancer to neoadjuvant chemotherapy. J Magn Reson Imaging 2016; 44: 1107-1115.
- [22] Ocaña A, Diez-Gónzález L, Adrover E, Fernández-Aramburo A, Pandiella A and Amir E. Tumor-infiltrating lymphocytes in breast cancer: ready for prime time? J Clin Oncol 2015; 33: 1298-1299.
- [23] Wu S, Berg WA, Zuley ML, Kurland BF, Jankowitz RC, Nishikawa R, Gur D and Sumkin JH. Breast MRI contrast enhancement kinetics of normal parenchyma correlate with presence of breast cancer. Breast Cancer Res 2016; 18: 76.
- [24] Liu Y, Wang S, Qu J, Tang R, Wang C, Xiao F, Pang P, Sun Z, Xu M and Li J. High-temporal resolution DCE-MRI improves assessment of intra- and peri-breast lesions categorized as BI-RADS 4. BMC Med Imaging 2023; 23: 58.
- [25] Li H, Zhu Y, Burnside ES, Huang E, Drukker K, Hoadley KA, Fan C, Conzen SD, Zuley M, Net JM, Sutton E, Whitman GJ, Morris E, Perou CM, Ji Y and Giger ML. Quantitative MRI radiomics in the prediction of molecular classifications of breast cancer subtypes in the TCGA/TCIA data set. NPJ Breast Cancer 2016; 2: 16012.
- [26] Waugh SA, Purdie CA, Jordan LB, Vinnicombe S, Lerski RA, Martin P and Thompson AM. Magnetic resonance imaging texture analysis classification of primary breast cancer. Eur Radiol 2016; 26: 322-330.
- [27] Li H, Zhu Y, Burnside ES, Drukker K, Hoadley KA, Fan C, Conzen SD, Whitman GJ, Sutton EJ, Net JM, Ganott M, Huang E, Morris EA, Perou CM, Ji Y and Giger ML. MR imaging radiomics signatures for predicting the risk of breast cancer recurrence as given by research versions of MammaPrint, oncotype DX, and PAM50 gene assays. Radiology 2016; 281: 382-391.
- [28] Wan T, Bloch BN, Plecha D, Thompson CL, Gilmore H, Jaffe C, Harris L and Madabhushi A. A radio-genomics approach for identifying high risk estrogen receptor-positive breast cancers on DCE-MRI: preliminary results in predicting OncotypeDX risk scores. Sci Rep 2016; 6: 21394.

- [29] Georgiou L, Wilson DJ, Sharma N, Perren TJ and Buckley DL. A functional form for a representative individual arterial input function measured from a population using high temporal resolution DCE MRI. Magn Reson Med 2019; 81: 1955-1963.
- [30] Cheng Z, Wu Z, Shi G, Yi Z, Xie M, Zeng W, Song C, Zheng C and Shen J. Discrimination between benign and malignant breast lesions using volumetric quantitative dynamic contrastenhanced MR imaging. Eur Radiol 2018; 28: 982-991.
- [31] Jena A, Taneja S, Singh A, Negi P, Mehta SB and Sarin R. Role of pharmacokinetic parameters derived with high temporal resolution DCE MRI using simultaneous PET/MRI system in breast cancer: a feasibility study. Eur J Radiol 2017; 86: 261-266.
- [32] Wang PN, Velikina JV, Bancroft LCH, Samsonov AA, Kelcz F, Strigel RM and Holmes JH. The influence of data-driven compressed sensing reconstruction on quantitative pharmacokinetic analysis in breast DCE MRI. Tomography 2022; 8: 1552-1569.
- [33] Pinker K, Helbich TH and Morris EA. The potential of multiparametric MRI of the breast. Br J Radiol 2017; 90: 20160715.
- [34] Zakaria R, Radon M, Mills S, Mitchell D, Palmieri C, Chung C and Jenkinson MD. The role of the immune response in brain metastases: novel imaging biomarkers for immunotherapy. Front Oncol 2021; 11: 711405.
- [35] Houser M, Barreto D, Mehta A and Brem RF. Current and future directions of breast MRI. J Clin Med 2021; 10: 5668.